HHS Public Access

Author manuscript

*Nat Metab*. Author manuscript; available in PMC 2021 September 15.

Published in final edited form as:

*Nat Metab*. 2021 March ; 3(3): 318–326. doi:10.1038/s42255-021-00356-0.

# Fasting-induced FOXO4 blunts human CD4+ T helper cell responsiveness

**Kim Han**[1,*], **Komudi Singh**[1,2,*], **Matthew J. Rodman**[1], **Shahin Hassanzadeh**[1], **Kaiyuan Wu**[1], **An Nguyen**[1], **Rebecca D. Huffstutler**[3], **Fayaz Seifuddin**[2], **Pradeep K. Dagur**[4], **Ankit Saxena**[4], **J. Philip McCoy**[4], **Jinguo Chen**[5], **Angélique Biancotto**[5,#], **Katherine E. R. Stagliano**[5], **Heather L. Teague**[6], **Nehal N. Mehta**[3,6], **Mehdi Pirooznia**[2], **Michael N. Sack**[1,3,§]

[1]Laboratory of Mitochondrial Biology and Metabolism, National Heart, Lung, and Blood Institute, National Institutes of Health, Bethesda, MD

[2]Bioinformatics and Computational Core Facility, National Heart, Lung, and Blood Institute, National Institutes of Health, Bethesda, MD

[3]Cardiovascular Branch, National Heart, Lung, and Blood Institute, National Institutes of Health, Bethesda, MD

[4]Flow Cytometry Core Facility, National Heart, Lung, and Blood Institute, National Institutes of Health, Bethesda, MD

[5]Center of Human Immunology, National Institute of Allergy and Infectious Diseases, National Institutes of Health, Bethesda, MD

[6]Laboratory of Cardiometabolic Disease and Inflammation, National Heart, Lung, and Blood Institute, National Institutes of Health, Bethesda, MD

## Abstract

Intermittent fasting blunts inflammation in asthma[1] and rheumatoid arthritis[2], suggesting that fasting may be exploited as an immune-modulatory intervention. However, mechanisms underpinning anti-inflammatory effects of fasting remain poorly characterized[3, 4, 5]. Here, we show that fasting in humans is sufficient to blunt $CD4^+$ T helper cell responsiveness. RNA-seq and flow cytometric immunophenotyping of peripheral blood mononuclear cells (PBMCs) from volunteers subjected to overnight or 24-hour fasting, and 3-hours of refeeding implicate that fasting blunts $CD4^+$ T helper cell activation and differentiation. Transcriptomic analysis reveal that the longer fast-duration has a more robust effect on $CD4^+$ T cell biology. Through bioinformatic analyses, we identify the transcription factor FOXO4 and its canonical target FKBP5 as a potential



§Address Correspondence To: Michael N. Sack (sackm@nih.gov), Laboratory of Mitochondrial Biology and Metabolism, NHLBI, NIH, Bldg. 10-CRC, Room 5-3342, 10 Center Drive, Bethesda, MD 20892, USA.

#AB – Current Address: Department of Precision Immunology, Sanofi, USA

Contributions

Conceived the project: KH, KS, MNS.; Secured Funding: MNS.; Designed the experiments: KH, KS, RDH, KERS, MP, MNS.; Carried out experiments: KH, KS, MJR, AN, SH, KW, RDH, AS, PD, AB, HT.; Analyzed data: KH, KS, FS, PD, AS, JC, HT.; Wrote the manuscript: KH, KS, MNS and edited Manuscript: MJR, JPM, KERS, NNM, MP.

*KH and KS contributed equally to this study.

Competing interests: None

fasting-responsive regulatory axis. Genetic gain- or loss-of-function of FOXO4 and FKBP5 is sufficient to modulate Th1 and Th17 cytokine production. Moreover, we find that fasting-induced or genetic overexpression of FOXO4 and FKBP5 is sufficient to downregulate mTORC1 signaling and suppress STAT1/3 activation. Our results identify FOXO4-FKBP5 as a novel fasting-induced, STAT-mediated, regulatory pathway to blunt human $CD4^+$ T helper cell responsiveness.

## Summary:

How fasting limits inflammation is poorly understood. RNA-seq analysis identified induction of the FOXO4-FKBP5 axis by fasting. Gain and loss of function studies in $CD4^+$ T cells shows that FOXO4 and FKBP5 levels mediate T helper cell responsiveness, in part, by reducing mTORC1 and STAT1/3 signaling.

---

To understand the impact of caloric exposure and fasting duration on immune system modulation, a clinical protocol was established to perform immune cell profiling in 28 healthy human subjects. The clinical protocol and the serological response to changes in the caloric load are depicted in Fig. 1a and Extended Data Fig. 1a, respectively. RNA sequencing was performed on PBMCs from 21 subjects following an overnight (baseline) and following a 24-hr. fast and 3 hrs. after refeeding. These time points were selected as a clear dichotomy in NLRP3 inflammasome and $CD4^+$ Th2 cell activation are evident, using this fasting/refeeding protocol in healthy volunteers and in steroid-naïve asthma[3, 6]. Gene expression quantification was followed by differentially expression (DE) and co-expression/subnetwork analysis. The initial analysis revealed numerous DE genes in the comparisons between the 3 groups (Extended Data Fig.1b). Unsupervised principal component analysis (PCA) of DE genes from all 3 comparisons showed that caloric exposure was the primary factor driving gene expression changes (Extended Data Fig.1c). Combined PCA analysis of the top 1000 DE genes from all 3 groups showed a similar discrimination between groups (Extended Data Fig.1d). In parallel, volcano plots showed significantly DE genes between the caloric load states (Fig. 1b) and pathway enrichment implicated that the most highly enriched gene sets encoded for proteins linked to T cell biology (Extended Data Fig.1e). Comparison of the refed group with baseline or 24-hr. fasting was assessed to evaluate the effect of fasting duration. The DE genes obtained comparing the refed state with either baseline or 24-hr. fasting revealed an ~50% overlap of DE genes from both comparisons (Fig. 1c). To understand the effect of fasting duration, we evaluated fold changes of overlapping DE genes of the two fasted states compared to refeeding. Interestingly, both the upregulated and downregulated DE genes were modulated to a greater extent following the 24-hr. *vs.* overnight fasting compared to refeeding (Extended Data Fig.1f–g). Pathway enrichment analysis and differential enrichment maps showed that the common 846 DE genes from two fasted states were enriched for T cell activation, differentiation and aggregation (Fig. 1d–e). Concurrently DE genes that were exclusively modulated by the 24-hr. fast significantly enriched in pathways related to endosome trafficking, ephrin signaling and vacuolar transport (Extended Data Fig.1h). Interestingly endosomal trafficking and vacuolar transport are integral for immune activation[7, 8] and ephrin signaling supports T cell proliferation, activation and migration[9]. These data suggested that longer fasting duration may have a sustained impact on expression of genes involved in T cell immunomodulation.

To evaluate whether these gene regulatory effects were mirrored by cell surface receptor signatures we screened PBMCs using high-dimensional flow cytometry immunophenotyping[10]. This analysis enabled quantitation of relative activation of PBMC subpopulations at baseline (overnight fast), 24-hr. fasting, and refeeding. Firstly, the overall PBMC cell population distribution was unchanged comparing caloric-load conditions (Extended Data Fig.2a). Analysis showed a general alignment of baseline and 24-hr. fasting cell surface markers compared to refeeding. Predominantly, and in parallel with the RNA-seq analysis, differentiation between fasting groups and refeeding was more pronounced following the 24-hr. fast (Fig. 2a–c and Extended Data Fig. 2). Gating strategies used to identify immune cell subsets are provided in Extended Data Fig. 2b (total and $CD4^+$ and $CD8^+$ T cell populations), Supplementary Table 2, and Supplementary Data 1–3. Comparing 24-hr. fasting to refeeding uncovered three distinct patterns: i) fasting reduced cell populations of activated monocyte, $CD4^+$ T and $CD8^+$ T cells and $CD4^+$ Th1, Th2 and Th17 signatures (Fig. 2a–c, Extended Data Fig.2c–d); ii) fasting increased markers of activated myeloid and plasmacytoid dendritic cells (Extended Data Fig.2e); and iii) fasting had no impact on Tregs, classical monocytes, $CD4^+$ T follicular helper cells, activated NK cells, immature and mature B cells, and $CD8^+$ Tc1 and Tc17 signatures (Extended Data Fig.2c and 2f–j). The cytometry measurements for surface markers were performed without *ex vivo* priming or activation to reflect *in vivo* physiologic effects. T cell activation was required to measure intracellular cytokine markers. Intracellular markers showed reduced IFNγ and IL-17 levels respectively in the 24-hr. fasted group, with no differences in IL-4 levels between 24-hr. fasting and refeeding (Fig. 2c).

Given enrichment of DE genes linked to T cell processes, and the flow data showing fasting effects on $CD4^+$ T helper cells, we evaluated caloric-load dependent $CD4^+$ T cell responsiveness. Naïve $CD4^+$ T cells were isolated from human subjects at the 3-caloric load timepoints and cultured with anti-CD3 and anti-CD28 antibodies to drive T cell receptor (TCR) activation. Consistent with the flow data, the Th1 and Th17 linked cytokines including IFNγ and IL-17 and IL-22 levels, were significantly reduced following the 24-hour fast and IL-22 was reduced at baseline compared to refeeding (Fig. 2d). Levels of the Th2 cytokines IL-5 and IL-13 were equally blunted in both fasting states compared to refeeding (Fig. 2e). To evaluate whether these fasting-refeeding differences were retained following T cell differentiation, $CD4^+$ T cells were incubated with lineage-distinct cytokine cocktails. The secretion of IFNγ in Th1, IL-5 in Th2, and IL-17 in Th17 differentiated cells were lower following 24-hr. of fasting *vs.* refeeding (Fig. 2f). In parallel, transcript levels of canonical transcription factors (TFs) driving these $CD4^+$ T cell fates, TBX21 (Th1), GATA3 (Th2) and RORC (Th17), were all significantly lower following 24-hrs. of fasting (Fig. 2g).

To identify potential mechanisms driving caloric-load mediated immune modulation, we employed weighted gene co-expression network analysis (WGCNA) to identify correlated gene clusters/module[11]. Twenty-two co-expression clusters were identified in the 24-hr. fasting and refed RNA-seq datasets (Extended Data Fig.3a). However, only a few fasting and refeeding datasets showed overlap suggesting distinct fasting and refeeding regulatory events (Extended Data Fig.3a). To refine clusters critical for caloric-load dependent regulation, overlap of DE genes with WGCNA clusters was evaluated. This identified five significant fasting clusters and seven significant refed clusters. Subsequent Cell type

enrichment (CTen) analysis was performed to evaluate whether specific clusters aligned with immune cell subpopulations[12]. Genes in two of 5 fasting, and four of 7 refed clusters enriched in $CD4^+$ T cell genes (Extended Data Fig. 4). A representative CTen of fasted cluster showed significant enrichment of $CD4^+$ T and $CD8^+$ T cell expressed genes (Extended Data Fig.3b).

To identify putative fasting mediated regulatory mechanisms, $CD4^+$ T cell enriched clusters were interrogated for pathway enrichment, and potential protein-protein interactions (PPI), and/or transcriptional factors (TF) networks. Interestingly genes in $CD4^+$ T cell linked fasting clusters enriched in intracellular trafficking, protein secretion processes; and genes in $CD4^+$ T cell linked refed clusters enriched in processes associated with RNA processing, T cell differentiation, viral genome replication, and adaptive immune responses (Extended Data Fig. 4). A significant PPI network involving HDAC5-GATA3-NFκB2 was identified (Extended Data Fig.3c and Extended Data Fig. 4) and overlaying gene expression fold change information on this network revealed that the HDAC5-GATA3-NFκB2 interactome, which are known to contribute to T cell activation[13, 14, 15], was reduced by fasting (Extended Data Fig.3c–d).

Additionally, a fasting module identified FOXO4, as a potential TF network with most of its targets increased by fasting (Fig. 3a and Extended Data Fig. 4). Concurrent in-silica analysis using the Find Individual Motif Occurrences (FIMO) tool[16] identified FOXO4 binding motifs in promoter regions of a significant proportion of fasted DE upregulated genes (Fig. 3b). To further explore the FOXO4 network RT-PCR was performed on target genes from RNA extracted from PBMCs. The FOXO4 controlled network pathway was predominantly increased with fasting as evident by increased transcript levels of genes encoding for FK506-binding protein 5 (FKBP5), FBXO32, and TXNIP and although transcript levels of DUSP6 and BCL6 were reduced (Fig. 3a). We then assessed FOXO4 protein levels in the different caloric-load conditions and showed that FOXO4 levels were significantly higher after 24-hr. fasting (Fig. 3c). To validate these findings, primary human $CD4^+$ T cells were extracted from a separate group of healthy volunteers and subjected to siRNA knockdown and lentiviral infection harboring FOXO4 or control expression vectors. Following knockdown, expression of FOXO4 was reduced by ≈ 60% (Extended Data Fig.3e–f) and in response to TCR activation, cytokine levels linked to Th1 and Th17 activation were significantly induced compared to the response in scrambled controls (Fig. 3d). Concordantly, FOXO4 transduction blunted IFNγ and IL-17 secretion (Fig. 3e, Extended Data Fig.3g). These gain and loss of function experiments support FOXO4 as a negative regulator of Th1 and Th17 T cell responsiveness.

Furthermore, as fasting activates AMPK and blunts mTORC1 signaling[17] we explored the impact of FOXO4 transduction on nutrient sensing signaling. FOXO4 transduction increased activated $CD4^+$ T cell AMPK phosphorylation and diminished mTOR, p70s6K, and S6 phosphorylation (Fig. 3f). Additionally, FOXO4 transduction blunted phosphorylation of the canonical T cell STAT regulatory proteins; STAT1 and STAT3[18] (Fig. 3g). In parallel, flow cytometric analysis confirmed that FOXO4 transduction reduced Th1 and Th17 cell surface markers (Fig. 3h) and blunted intracellular IFNγ, IL-17 and IL-4 cytokine expression (Fig. 3i).

To explore additional downstream effects of fasting-induced FOXO4 expression, we confirmed that transcript levels of FOXO4 target genes initially identified as being increased in fasting (Fig. 3a) were induced by FOXO4 overexpression. In parallel with fasting, FOXO4 increased FKBP5, FBXO32 and TXNIP transcript levels (Fig. 4a). Interestingly, partial least squares discrimination analysis (PLS-DA) of RNA-seq data from all 3 groups identified FKBP5 as a top variable importance in prediction (VIP) gene to discriminate between refeeding and both fasting states (Extended Data Fig. 5a). In alignment with this, FOXO4 overexpression increased FKBP5 protein levels (Fig. 4b), and FKBP5 transduction blunted IFNγ and IL-17 secretion (Fig. 4c and Extended Data Fig.3h) and reduced mTOR and STAT1 phosphorylation (Fig. 4d–e). In addition, FKBP5 overexpression blunted protein levels of master TFs driving $CD4^+$ T cell fate, TBX21 (Th1) and RORC (Th17) (Extended Data Fig. 5b). To validate FKBP5 function, primary human $CD4^+$ T cells were subjected to siRNA knockdown and in response to TCR activation, IFNγ and IL-17 cytokine levels were significantly induced compared to the response in scrambled controls (Extended Data Fig. 5c–d). These gain and loss of function experiments support that FKBP5, like FOXO4, mediate Th1 and Th17 cell responsiveness.

As the myeloid cell immunomodulatory effect of 24-hr. fasting in humans could be replicated in mice following a 48-hr. fast[3, 19], we assayed if this prolonged murine fast could mirror human $CD4^+$ T cell responsiveness. In parallel with the human data fasted mouse $CD4^+$ T cells showed FOXO4 and FKBP5 induction (Fig. 4f) with diminished release of IFNγ and IL-17 (Fig. 4g).

Immune cell differentiation and responsiveness to infections/injury are orchestrated by a large number of transcription factors and their interaction and control are both intricate and complex[20, 21, 22, 23]. This study augments our understanding of immune regulatory control by identifying FOXO4 as caloric-load responsive and implicates its role in fasting mediated modulation of the $CD4^+$ T cell lineage propensity. FOXO4 is a member of the Forkhead box O (FOXO) TF family, and these TFs are usually negatively regulated by insulin signaling. This pattern of expression supports induction of FOXO4 in the fasted state, where insulin levels are reduced.

In mice, three members of the FOXO family (FOXP3, FOXN1 and FOXJ1) have been clearly linked to T cell biology[24] and FOXP3 is essential for the differentiation, maintenance and immunosuppressive function of regulatory T cells[25]. FOXO4 has been less well characterized, although it has been shown to inhibit NF-κB, and FOXO4 null mice exhibit increased susceptible to chemical colitis with excess $CD4^+$ T cell infiltration and elevated IFNγ[26]. Our findings expand this understanding by showing that FOXO4 levels are increased in the fasted state and that genetic modulation of FOXO4 levels modulate Th1 and Th17 cell regulation. Bioinformatic analyses suggested that FOXO4 may function, in part, via the upregulation of FKBP5. The induction of FKBP5 in $CD4^+$ T cells, recapitulated both the fasting effect and the effects of the genetic manipulation of FOXO4 levels. Interestingly, FKBP5 has been shown to be largely restricted to T cells[27] and has been shown to have context specific effects on the modulation of T cell activation[27, 28]. FKBP5 functions as a cochaperone protein and its intrinsic role, independent of FK506 or cyclosporin A administration[27], require further exploration. Emerging studies supports its role in the

inhibition of glucocorticoid receptor signaling and in the activation of PPARγ and downstream pathways[29]. Together, these gain and loss of function experiments support FOXO4/FKBP5 as negative regulators of Th1 and Th17 T cell responsiveness. It is likely that other signaling pathways may be involved in modulating the Th2 subset.

A study limitation is that the RNA-seq was performed on PBMCs versus single cell populations which diminishes the capacity to identify regulatory events in less prevalent PBMC populations or in T cell subsets. Concurrently, pathway enrichment analysis also supports that fasting and refeeding additional modulates myeloid and B cell biology, which warrant exploration. Additionally, it is probable that both cell intrinsic and paracrine effects contribute to the caloric-load dependent gene regulatory effects, in part, due to paracrine contributions from, for e.g., adipocytes, skeletal muscle and the liver in response to fasting. These effects similarly require examination.

In conclusion, in this study we interrogated the gene expression profile of PBMCs in response to physiologic nutrient stressors to identify pathways controlling caloric load mediated immune modulation. The composite of bioinformatic analyses showed that the 24-hr. fast has more robust effects on genes controlling immune regulation compared to overnight fasting. Combined RNA-seq and flow cytometry analysis in human PBMCs and subsequent candidate pathway characterization in human and mouse $CD4^+$ T cells identified the FOXO4-FKBP5 axis as a regulatory pathway facilitating fasting mediated blunting of $CD4^+$ T cell responsiveness. Although fasting itself confers a broader array of immunomodulatory effects, when focused on Th cell biology, FOXO4 and FKBP5 appear to blunt Th1 and Th17 responsiveness via suppression of mTORC1 and STAT1/3 signaling. Further exploration of these regulatory pathways should advance our understanding how fasting and fasting mimetics confer ameliorative effects on inflammation.

## Methods

### Study Design and Subjects

This fasting and refeeding pilot study was registered in ClinicalTrials.gov with the registration number NCT02719899 and approved by the National Heart and Lung Institute IRB. Subjects were screened in the ambulatory clinic and signed informed consent for the protocol prior to undertaking the study (Visit 1). Subjects initiated the study after an overnight fast with blood draw for the baseline immune response (Visit 2). After overnight fasting the study subjects consumed a fixed 500 calorie meal before 8am in the morning and fasted for 24 hours except for unrestricted water intake. Following a 24-hr. fasting blood draw (Fasting-Visit 3), the subjects ate another 500-calorie meal with post-prandial blood draws 3 hours later (Refed-Visit 3). The schematic of the blood draw protocol is shown in Fig. 1a. The subject group consisted of 16 females and 12 males with an age range from 21 to 32 years (means ± SD: 24.6 ± 2.6) and had 22–29 BMI range (means ± SD: 24.6 ± 2.1). All these subjects had no history of acute or any chronic disease. Subjects had a choice between 2 isocaloric breakfasts: option 1) vegetable omelet, toast with butter and jelly, and orange juice; option 2) oatmeal with walnuts, brown sugar, dried cranberries and milk. The blood from healthy volunteers for functional validation of transcription factors were

obtained from subjects that consented to enroll on the Disease Discovery Protocol (NCT01143454) and from the NIH Clinical Center blood bank (NCT00001846).

## Cell Culture and Transfection

Primary PBMCs were isolated from human blood by density centrifugation using Lymphocyte Separation Medium (MP Biomedicals). PBMCs were preferentially used for immune function experiments and cryopreserved by Planer 750Plus Controlled Rate Freezer (Planer PLC) for flow cytometry. $CD4^+$ T cells were negatively selected (>95% purity) from PBMCs using the $CD4^+$ T Cell Isolation Kit (Miltenyi Biotec) and cultured in RPMI 1640 media supplemented with 25 mM HEPES, 10% heat-inactivated FBS, and Penicillin/Streptomycin. For knockdown experiments, $CD4^+$ T cells were isolated from healthy volunteers and Accell control siRNA, SMARTpool Accell FOXO4 siRNA, and SMARTpool Accell FKBP5 siRNA (Dharmacon) were transfected with Accell siRNA delivery media or T cell Nucleofector kit according to manufacturer's instruction (Lonza). To increase cell viability, $CD4^+$ T cells were incubated in media supplemented with 50 ng/ml IL-2 (Peprotech) for 24 hours after transfection and then activated with plate-coated 5 μg/ml αCD3 (BioLegend) and 10 μg/ml αCD28 (BioLegend) for 3 days. To produce lentivirus, pLenti vector, pLVX-IRES-GFP, pLenti-FOXO4 with Myc-DDK tag (Origene Technologies), pLVX-GFP-IRES-FKBP5, and packing plasmids (psPAX2 and pMD2.G from Addgene) were transfected into 293T cells using Polyjet reagent (Signagen Laboratories). Supernatants were collected 48 hours after transfection, filtered through a 0.45 μm syringe filter and concentrated by ultracentrifugation at 25,000 rpm for 2 hours. Virus was introduced into the $CD4^+$ T cell culture media in the presence of 8 μg/ml of DEAE-dextran (Sigma) and incubated in the presence of 50 ng/ml IL-2 for 24 hours before TCR activation.

## Cell Stimulation and Cytokine Assays

Human $CD4^+$ T cells ($3\times10^5$/well in 96-well plate) were activated with plate-coated αCD3 (5 μg/ml, BioLegend) and αCD28 (10 μg/ml, BioLegend) for 3 days in the presence of 10% fasted or refed serum from the subjects and 5% heat-inactivated FBS. Also, $CD4^+$ T cells ($2\times10^5$/well in 96-well plate) were differentiated into three T cell subtypes by incubation with the specific supplements for Th1 (20 ng/ml IL-12 and 10 μg/ml αIL-4), Th2 (10 ng/ml IL-4 and 10 μg/ml αIFNγ) or Th17 (20 ng/ml IL-6, 2 ng/ml TGF-β1, 10 ng/ml IL-1β, 10 ng/ml IL-23, 10 μg/ml αIL-4, and 10 μg/ml αIFNγ), respectively. They were differentiated for 3 days on plate-coated αCD3 and αCD28 in the presence of 10% fasted or refed serum from the subjects. All recombinant proteins and antibodies for differentiation media were purchased from Peprotech and eBioscience. Supernatants were collected, centrifuged to remove cells and debris, and stored at −80°C. The levels of cytokines, including IFNγ, IL-5, IL-13, IL-17, and IL-22 were measured by ELISA (R&D Systems). Results were normalized to cell number using the CyQuant cell proliferation assay (Invitrogen) or BCA protein assay (Pierce).

## Animal studies

Mice were kept under specific pathogen-free conditions and provided with food and water ad libitum. Animal experiments were approved by the NHLBI, National Institutes of Health

Animal Care and Use Committee (Animal Protocol H0222R3). Male mice at 4–7 months of age in the C57BL/6 background (Jackson Laboratory, Stock No. 000664) were fed or fasted for 48 hrs. Mice were fed rodent chow pellets (LabDiet, Cat. No. 5021). Mouse $CD4^+$ T cells were negatively selected (>95% purity) from splenocytes using the $CD4^+$ T Cell Isolation Kit (Miltenyi Biotec) and cultured in RPMI 1640 media supplemented with 25 mM HEPES, 10% heat-inactivated FBS, and Penicillin/Streptomycin. For cytokine measurement $CD4^+$ T cells ($4\times10^5$/well in 96-well plate) were activated with 500 ng/ml PMA and 1 μg/ml Ionomycin for 4–6 hrs. For immunoblot analysis $CD4^+$ T cells ($2\times10^6$/well in 12-well plate) were incubated on plate-coated αCD3 (10 μg/ml, BioLegend) and αCD28 (10 μg/ml, BioLegend) for 24 hrs.

## Blood Biochemical Assays

Blood was collected after 24-hr. fasting and refeeding for standard laboratory testing in the Department of Laboratory Medicine, NIH Clinical Center. Standard laboratory tests included the measurement of glucose (Glucose HK Gen 3, Roche Diagnostics), insulin (Elecsys Insulin cobas e analyzer, Roche Diagnostics) and growth hormone (Siemens Immulite 2000 XPi GRH, Siemens) levels.

## RNA-seq Library Preparation and Data Analysis

PBMCs from the same 21 subjects PBMCs were used for flow cytometry and RNA-seq. RNA was extracted from PBMCs by miRNeasy Micro Kit (Qiagen). RNA was quantified using a Qubit 3.0 fluorometer (Thermo Fisher Scientific) and its integrity confirmed using an Agilent Technologies 2100 Bioanalyzer (Agilent). Dual index libraries were constructed with at least one unique index per each library using TruSeq Stranded Total RNA HT Kit (Illumina), to enable subsequent pooling of equal quantities of individual libraries. The integrity and ratio of pooled libraries was validated using Miseq system (Illumina) and then paired-end sequencing (2×75 bp) was performed on an HiSeq3000 sequencer (Illumina), with the Illumina HiSeq3000 SBS kit. The RNA sequence data obtained from the libraries (bcl2fastq software (version 2.17, Illumina) was subjected to quality control (FastQC, a quality control tool for high throughput sequence data and available online at: http://www.bioinformatics.babraham.ac.uk/projects/fastqc), and trimmomatic (0.33; https://github.com/timflutre/trimmomatic) to remove adapters, followed by quality trimming (trimmomatic tool, V0.33; https://github.com/timflutre/trimmomatic) and alignment to the human genome (GRCh38) using HISAT2.40 (https://daehwankimlab.github.io/hisat2/)[30]. Gene expression levels were quantified using Stringtie (https://github.com/gpertea/stringtie)[30, 31] and differentially expressed genes were evaluated using Ballgown (http://bioconductor.org/packages/release/bioc/html/ballgown.html)[32]. The differentially expressed genes was further subjected to pathway enrichment analysis using ClusterProfiler (https://bioconductor.org/packages/release/bioc/html/clusterProfiler.html)[33]. All the codes can be found here: https://github.com/NHLBI-BCB/PTNA. For WGCNA analysis (https://cran.r-project.org/web/packages/WGCNA/index.html), genes with expression >1 FPKM in 90% of the samples were selected from 24-hr. fasting and refed RNA seq expression datasets. The filtered RNA seq data was used to generate co-expressing genes modules using weighted gene co-expression network analysis (WGCNA)[11]. Subnetwork analysis of the co-expressing gene modules was performed using GeneMANIA[34] physical interaction database

search in Cytoscape (V3.7.2; http://cytoscape.org/)[35]. The pathway enrichment graphical summary was generated in Cytoscape using Enrichment Map and Auto Annotate plugins. The gene expression fold change information was overlaid on the gene networks using Cytoscape. GeneNet Toolbox (http://avigailtaylor.github.io/gntat14)[36] was used to determine the significance of connectivity using network permutation and the p value < 0.05 of the significant networks are reported. Additionally, DE genes (from 24-hr fasting to refeeding comparison) that may potentially be FOXO4 transcription factor target were identified using the Find Individual Motif Occurrences (FIMO, http://meme-suite.org/doc/fimo.html) tool[16]. For this analysis, 1000 bp nucleotide sequence upstream of the transcription start site of each of the DE genes were used for scanning the FOXO4 binding motif. Finally, the partial least squares discrimination analysis (PLS-DA; https://bioconductor.org/packages/mixOmics/) of RNA-seq data from all 3 groups identified the variable importance in prediction (VIP) gene to discriminate between refeeding and both fasting states.

## High-dimensional Flow Cytometry Immunophenotyping

PBMCs from 21 subjects were used for flow cytometry. Two subjects' data were excluded from flow analysis due to red blood cell contamination of the samples. 10-color flow cytometry using five customized panels (T, B, $CD4^+$ helper T (Th), Regulatory T (Treg), and Natural killer (NK)/Dendritic cells (DC's)/Monocytes) and 18-color panel was designed to allow deep immunophenotyping of the predominant cell populations found in human PBMCs. PBMCs were thawed in FACS buffer (PBS with 0.25 mM EDTA and 0.1% BSA) and approximately $5–10\times10^6$ cells were stained with antibodies listed in Supplementary Table 1 (BD Lyoplate stain 175 including T cell cocktail, B cell cocktail, Helper T cell cocktail, Treg cocktail, and DC/Monocytes/NK cell cocktail and 18-color panel) followed by LIVE/DEAD Fixable Yellow stain (Invitrogen). Data were acquired with LSR Fortessa (BD). Post-acquisition analysis was performed using Flowjo 9.9.6 (Treestar Inc.). Analysis excluded debris and doublets using light scatter measurements, and dead cells by live/dead stain. Gating strategies used to identify immune cell subsets are provided in Supplementary Table 2 and Supplementary Data 1–3. $CD4^+$ T cells were isolated from healthy volunteers and transduced with control lentivirus and FOXO4 lentivirus. The cells were first gated for singlets (FSC-H *vs.* FSC-A) and further analyzed for their uptake of the Live/Dead Yellow stain to determine live versus dead cells in $CD4^+$ helper T (Th) panel (Extended Data Fig. 2b). $CD4^+$ T cells ($CD3^+CD4^+$) were gated for lymphocytes ($CD45^+$) and their expression of surface markers (CXCR3, CCR6, and CD294) is then determined within this gated population. For intracellular stain, PBMCs were activated with Cell stimulation cocktail plus protein transport inhibitors (eBioscience) and PMA (500 ng/ml, Sigma) for 3 hrs. Wilcoxon paired test was performed by a blinded investigator.

## Quantitative PCR Analysis

Total RNA was isolated using Nucleospin RNA kit (Macherey-Nagel) or miRNeasy Micro Kit (Qiagen). cDNA was synthesized with 500 ng of RNA using a first-strand synthesis kit (Invitrogen). Quantitative real-time PCR was performed using SYBR green PCR master mix (Roche) and run on Light cycler 96 systems (Roche, version 1.1). The primers of canonical transcription factors (TFs) were made by Integrated DNA Technologies and the sequences of the primers are listed; TBX21 (F: CGTGACTGCCTACCAGAAT and R:

ATCTCCCCCAAGGAATTGAC), GATA3 (F: GAACCGGCCCCTCATTAAG and R: ATTTTTCGGTTTCTGGTCTGGAT), RORC (F: GCATGTCCCGAGATGCTGTC and R: CTGGGAGCCCCAAGGTGTAG), and EF1α (F: GTTGATATGGTTCCTGGCAAGC and R: GCCAGCTCCAGCAGCCTTC) KEY RESOURCES TABLE. The transcript levels of other targets were measured using validated gene-specific QuantiTech primers (Qiagen). Relative gene expression was quantified by normalizing Ct values with 18S or EF1α using the $2^{-\Delta Ct}$ cycle threshold method.

## Immunoblot Analysis

Total proteins were extracted using RIPA buffer (50 mM Tris-HCl, pH 8.0, 0.5% deoxycholic acid, 1% NP-40, 0.1% sodium dodecyl sulfate and 0.5 M NaCl) supplemented with protease inhibitor cocktails and phosphatase inhibitors (Pierce). Protein concentration was measured using BCA protein assay (Pierce). The lysates were separated by NuPAGE Bis-Tris gel (Invitrogen) and transferred to nitrocellulose membranes (Bio-Rad). Membranes were incubated in Blocking buffer (Li-Cor) for 30 min at room temperature; primary antibody (1:1000 dilution) at 4°C overnight; and then secondary antibody (1:10000 dilution) conjugated with IRDye 800CW or IRDye 680RD (Li-Cor) for 1 hour at room temperature. Immunoblots were scanned using an Odyssey Clx imaging system (Li-Cor Biosciences) and protein band intensity was measured using Image studio software (version 5.2). Each phosphokinase is paired with its steady-state control protein and loading is validated by actin levels. Antibodies were purchased from Cell Signaling (FOXO4, FKBP5, pAMPKα (T172), AMPK, pmTOR (S2448), mTOR, pP70S6K (T389), P70S6K, pS6 (S240/244), S6, pSTAT1 (Y701), STAT1, pSTAT3 (Y705), STAT3, pSTAT6 (Y641), STAT6, TBX21, GATA3), ThermoFisher Scientific (RORC), Abcam (FOXO4), and Millipore (Actin).

The unprocessed immunoblots are provided in Source Data.

## Quantification and Statistical Analysis

Statistical analyses were performed using PRISM (GraphPad Software, version 8.4.1) and R (R Core Team (2019). R: A language and environment for statistical computing. R Foundation for Statistical Computing, Vienna, Austria. URL https://www.R-project.org/). For *in vivo* and *in vitro* studies, n represents the number of biological replicates per group and is reported in the Figure Legends. For histograms, means ± SEM for indicated number of observations are reported. The box plots show the median and upper/lower quartile of the observation. The whiskers show Turkey distribution and the outlier levels are shown as individual points. The dot and line plots show mean value of each subject. Statistical significance between two groups was determined using a two-tailed Student's t-test and paired Wilcoxon test when analyzing the response between groups. Overlap of DE genes with WGCNA modules were analyzed using the Fisher's exact test with $p$ value < 0.05 was considered significant. The paired Wilcoxon test was used to determine statistical significance when cytokines were measured from samples collected from the same subjects at different time points and for FACS analysis. For pathway enrichment results, $q$ value <0.05 (after correcting for multiple testing) is reported, otherwise $p$ values < 0.05 was considered statistically significant.

## Data and Code Availability

mRNA-seq datasets and data linked to study subjects BMI and sex is accessible in the GEO database- https://www.ncbi.nlm.nih.gov/geo/query/acc.cgi?acc=GSE165149. All the codes can be found here: https://github.com/NHLBI-BCB/PTNA.

## Reporting Summary

Further information on research design is available in the Nature Research Reporting Summary linked to this article.

# Extended Data

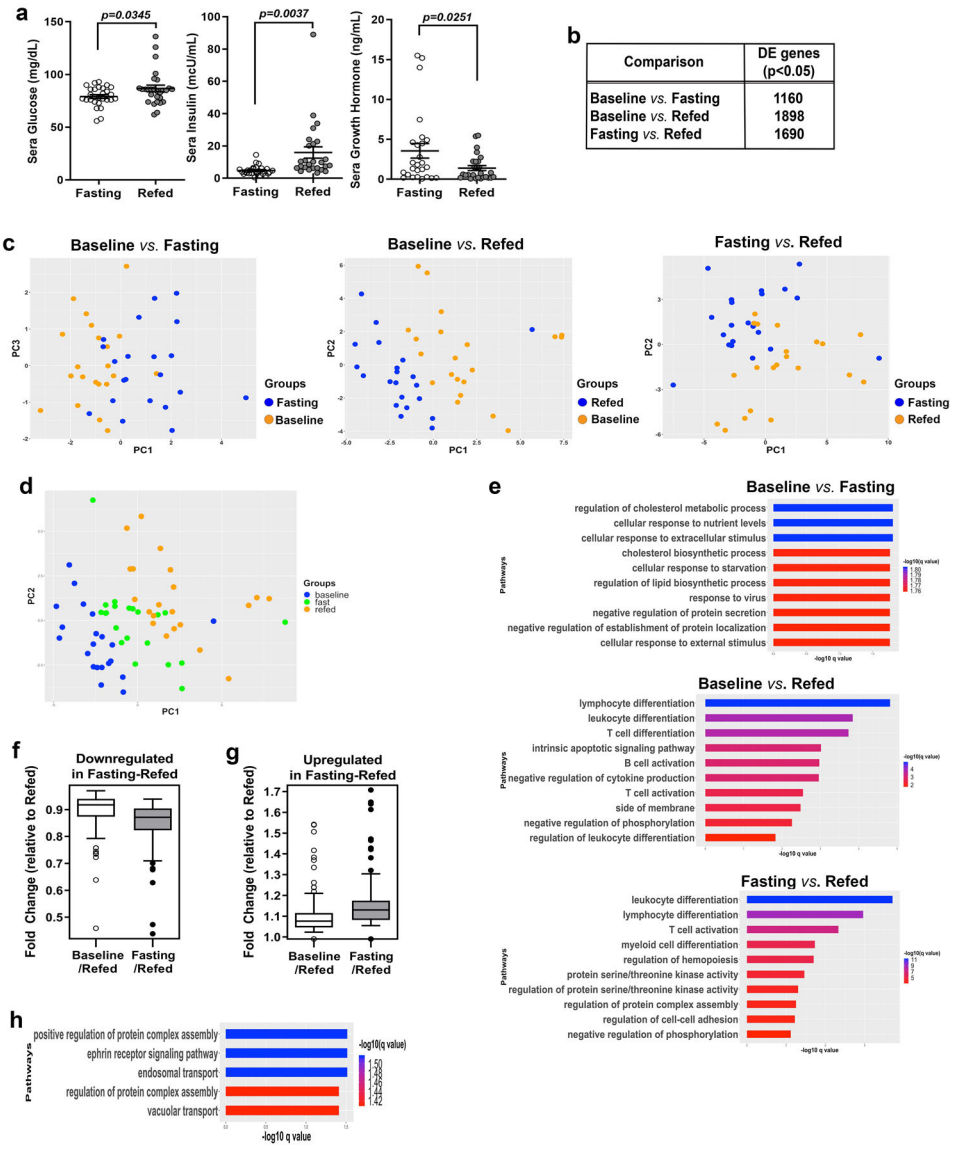


**Extended Data Figure 1. Initial analysis of RNA-seq data acquired from the 3 nutritional-load conditions.**

**a**, Individual points (symbols) and means±SEM (lines) of glucose, insulin and growth hormone levels following 24-hr. fasting and 3-hrs. following a fixed caloric meal. Dot plots represent mean±SEM with value of each subject (n=26–28 subjects). The values represent average of duplicates. Two-sided, paired Student's t-tests. Sera glucose (n=28), Sera insulin (n=26), Sera growth hormone (n=26). **b**, Table showing number of DE genes ($p<0.05$) identified in the indicated comparisons. PBMCs' RNA from 21 subjects used to generate RNA-seq data. **c**, Unsupervised principal component analysis (PCA) performed on DE genes ($p<0.05$) for indicated comparisons (n=21 subjects). **d**, Combined PCA analysis of the top 1000 DE genes ($p<0.05$) from all 3 groups. **e**, Top 10 pathways in which the DE genes ($p<0.05$) from the indicated comparisons. The q values (p values adjusted for false discovery rate (FDR)) from the enrichment result are represented by negative log10 scale (x axis). The most significant pathways predominantly align with lymphocyte and T cell differentiation and activation comparison with refed state. **f-g**, Box and whisker plots show range of fold change of the subset of 114 DE genes ($p<0.05$, RNA-seq analysis) that were either downregulated (**f**) or upregulated (**g**) to a greater degree following the 24-hr. fast *vs.* refeeding than baseline (overnight fast) *vs.* refeeding. The box and whiskers plots show median and upper/lower quartile of the relative gene expression. The whiskers show Turkey distribution and the outlier levels are shown as individual genes (n=21 subjects). **h**, Pathway enrichment analysis of 844 DE genes exclusively identified in the 24-hr. fasted versus refed state shown with q values (p value adjusted for FDR) for each pathway represented by negative log 10 scale (x axis). Statistical Source Data of Extended Data Fig. 1

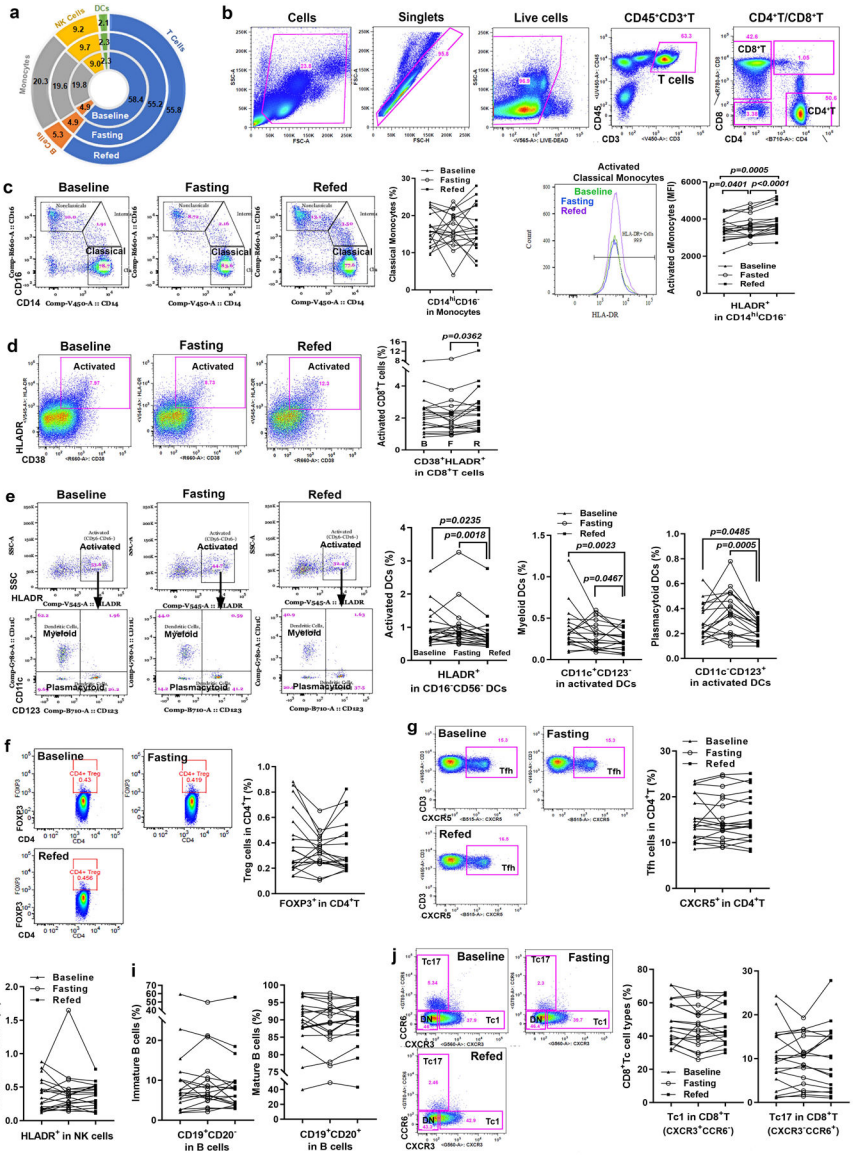

**Extended Data Figure 2. Flow cytometry using PBMCs exhibit differential fasting and refeeding cell-surface receptor expression levels.**

**a**, Nutrient-load dependent CD45$^{+}$ PBMC flow cytometry distribution. Schematic representation of cytometric labelling to distinguish cell type distributions at baseline, following 24-hr. fasting and refeeding (n=19 subjects). **b**, Cytometric plots and gating strategies to measure cell surface markers on T helper cells. **c-j**, Dot and line plots show cell populations of each subject (Wilcoxon two-sided, paired analysis to compare groups, n=19 subjects). **c**, Flow plots of activated classical monocytes from representative subject comparing 3 nutrient conditions. The plots show relative cell population frequencies of classical monocytes (CD14$^{high}$CD16$^{-}$) and median fluorescence intensity (MFI) of activated classical monocytes (HLADR$^{+}$ in CD14$^{high}$CD16$^{-}$). **d**, Representative flow plots showing gating and quantitation of activated CD8$^{+}$ T cells. Plots show expression of activated CD8$^{+}$ T cells (CD38$^{+}$HLADR$^{+}$ in CD8$^{+}$) showing significant increases in refed samples compared to baseline and fasting. **e**, Dot and line plots showing significant blunting in refed samples

compared to baseline and fasting in activated DCs (HLADR$^+$ in CD16$^-$CD56$^-$), myeloid DCs (CD11c$^+$CD123$^-$) and plasmacytoid cells (CD11c$^-$CD123$^+$). **f**, Representative flow plots showing gating and quantitation of regulatory T cells and plots show no difference in Treg cells (FOXP3$^+$). **g**, Follicular helper T cell (CD4$^+$CXCR5$^+$) levels show no difference in three caloricload conditions. **h**, Plots showing no difference in activated NK cells (HLADR$^+$ in CD16$^-$CD56$^+$, CD16$^+$CD56$^+$, and CD16$^+$CD56$^-$). **i**, Plots showing no difference in immature B cells (CD19$^+$CD20$^-$) and mature B cells (CD19$^+$CD20$^+$). **j**, Quantifying relative cell population frequencies with specific CD8$^+$ T (Tc) markers. Cell populations of Tc1 (CXCR3$^+$CCR6$^-$) and Tc17 (CXCR3$^-$CCR6$^+$) cells show no change in three caloric-load conditions. The antibody information of BD lyoplate and 18-color panel and gating strategy of flow cytometry is shown in Supplementary Tables 1 and 2 and Supplementary Data3.

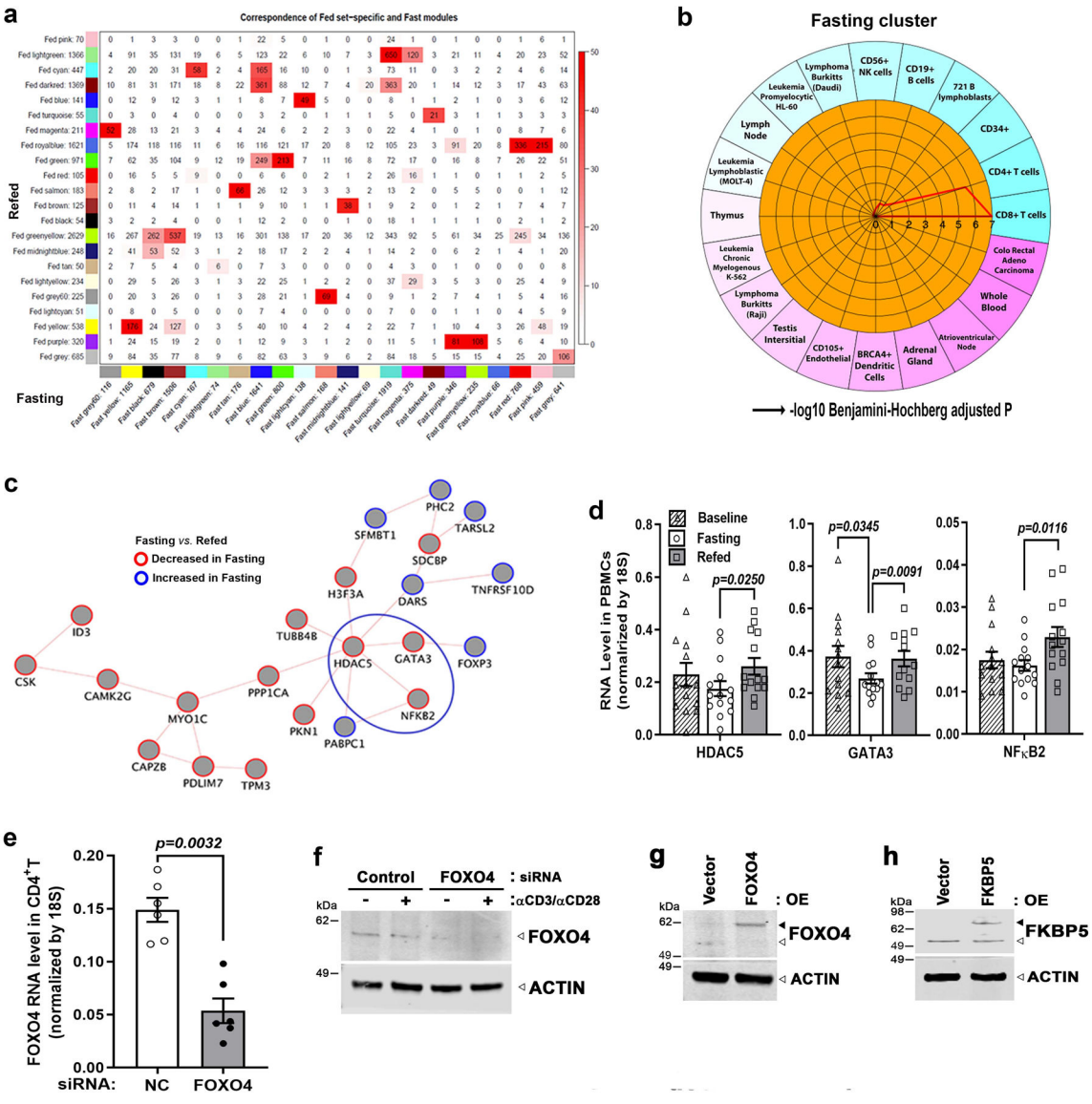

**Extended Data Figure 3. Weighted Gene Co-expression Network Analysis (WGCNA) identifies distinct and coordinate gene expression patterns in the fasting and refed states.**

**a**, Modules of genes with correlated expression patterns were clustered using WGCNA. The modules, with their distinct color designations using the fasted and refed data are shown on the x and y axes. Numerical assignment aligned to module colors represent number of genes per module. The correlated modules from fasting and refed were aligned to determine gene overlap (significance of the overlap determined by Fisher's exact test where red shading denotes significance - darker shade > significance). **b**, Representative cell type enrichment analysis (CTen) result of a fasting cluster showing enrichment of $CD8^+$ and $CD4^+$ T cells encoding genes (p-value depicted by red geometric plot extending from the center of the figure towards enriched cell types – representing −log10 Benjamini-Hochberg adjusted P. **c**, GeneMANIA derived protein-protein interaction (PPI) networks. Significant DE genes fold change information where blue circles represent increased, and red circles decreased expression during fasting compared to refeeding. **d**, qRT-PCR validation of selected network genes. Bar graph represent mean±SEM with value of each subject (n=14 subjects following 3–4 replicates using two-sided paired Student's t-test). **e**, Relative FOXO4 RNA expression in $CD4^+$ T cells in response to siRNA (Bar graph represent mean±SEM, n=6 health volunteers, two-sided, paired Student's t-test). **f**, Representative protein blot show FOXO4 expression in FOXO4-siRNA treated $CD4^+$ T cells from healthy subjects (n=3), 3 days following TCR activation (+). **g-h**, Representative immunoblots showing expression levels of (**g**) FOXO4- and (**h**) FKBP5-overexpression in $CD4^+$ T cells from healthy subjects (n=3). Open arrowheads - endogenous protein bands, overexpressed tagged-proteins - solid arrowheads. Source Data Extended Data Fig.3: Unprocessed immunoblots.

| Modules | CTen* | ClusterProfiler analysis (FDR<0.05) | PPI†/TF§ |
|---|---|---|---|
| **Fasting module** | | | |
| Cluster 1<br>Brown | $CD4^+$ T cells<br>$CD8^+$ T cells | Golgi to endosome transport<br>Methylation<br>Protein localization to Golgi apparatus | PPI: GAN interacting proteins (p value: 0.001)<br>TF: FOXO4 |
| Cluster 2<br>Midnightblue | $CD14^+$ Monocytes<br>$CD33^+$ Myeloid cells | Intrinsic apoptotic signaling pathway<br>Positive regulation of proteolysis<br>Regulation of cysteine-type endopeptidase activity | |
| Cluster 3<br>Salmon | WBC | Platelet degranulation<br>Regulated exocytosis<br>Blood coagulation | |
| Cluster 4<br>Tan | $CD19^+$ B cells<br>Tonsil<br>Lymphoma Burkitts | B cell activation | |
| Cluster 5<br>Blue | $CD4^+$ T cells<br>$CD8^+$ T cells | Lipid modification<br>Negative regulation of protein secretion<br>Negative regulation of hormone secretion | |
| **Refed module** | | | |
| Cluster 1<br>Red | $CD4^+$ T cells<br>$CD8^+$ T cells | Protein polyubiquitination<br>RNA splicing<br>Proteasomal protein catabolic process | |
| Cluster 2<br>Midnightblue | $CD14^+$ Monocytes<br>$CD33^+$ Myeloid cells | Apoptotic mitochondrial changes | |
| Cluster 3<br>Green | $CD4^+$ T cells<br>$CD8^+$ T cells<br>Adrenal cortex | Electron transport chain | |
| Cluster 4<br>Brown | $CD33^+$ Myeloid cells<br>$CD4^+$ T cells<br>Whole blood | No significant pathway enrichment | PPI: PKCα and MARCKS interactome (p value: 0.01) |
| Cluster 5<br>Greenyellow | WBC | Platelet degranulation<br>Blood coagulation, Coagulation | |
| Cluster 6<br>Blue | $CD56^+$ NK cells<br>$CD105^+$ Endothelial | Endosome to lysosome transport<br>Lysosomal transport<br>Ribosome biogenesis | PPI: NFκB interacting network and Neddylation protein interacting complex (p value: 0.03) |
| Cluster 7<br>Turquoise | $CD4^+$ T cells<br>$CD8^+$ T cells | Adaptive immune response<br>T cell differentiation<br>Viral genome replication | PPI: T cell activation (p value: 0.001)<br>TF: GATA4, PU.1, CEBPα |

**Extended Data Figure 4. Fasting and refed modules identified by WGCNA analysis.**

*CTen, Cell type enrichment; †PPI, Protein-protein interactions; §TF, Transcription factors

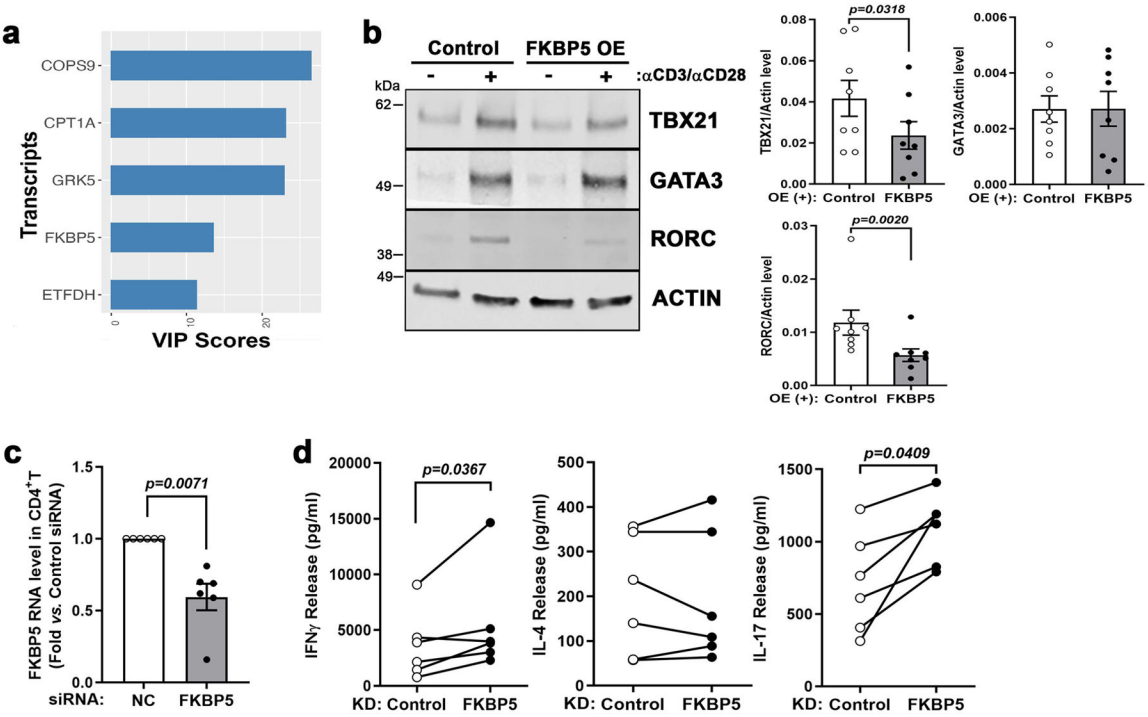


**Extended Data Figure 5. Evaluating FKBP5 effect on T cell activation.**

**a**, Top 5 variable importance in prediction (VIP) genes by partial least squares discrimination analysis (PLS-DA) of RNA-seq data from three caloric-load conditions. **b**, Representative protein blots and quantitative changes normalized by Actin of canonical TFs of Th1 (TBX21), Th2 (GATA3), and Th17 (RORC) in FKBP5-overexpression (OE) in $CD4^+$ T cells isolated from healthy volunteers, 3 days following TCR activation. Bar graph represent mean±SEM with data point of each health volunteer (n=8 subjects, Wilcoxon two-sided, paired analysis). **c-d**, $CD4^+$ T cells were isolated from healthy volunteers and transfected with FKBP5 siRNA and scrambled controls. **c**, Relative FKBP5 RNA expression in $CD4^+$ T cells (Bar graph represent mean±SEM with normalized value to scrambled control, n=6 subjects, values represent average of quadruplicates, two-sided, paired Student's t-test). **d**, Cytokine release of IFN**γ**, IL-4 and IL-17 following FKBP5 knockdown (KD) in $CD4^+$ T cells isolated from healthy volunteers, 3 days following TCR activation. The dot and line graphs represent mean value of each subject (n=6 biologically independent subjects, values represent average of duplicates, two-sided, ratio paired Student's t-tests). Source Data Extended Data Fig. 5: Unprocessed immunoblots.

## Supplementary Material

Refer to Web version on PubMed Central for supplementary material.

## Acknowledgements

This work was supported by the Intramural Research Program of the NHLBI of the National Institutes of Health. We thank Jessica Mann and Rongye Shi in the Center of Human Immunology, NIAID for the assistance with project management and sample collection, respectively. We thank and acknowledge the assistance of the NHLBI

DNA Sequencing and Genomics Core in performing the RNA library sequencing. **Trial Registration**: ClinicalTrials.gov ID: NCT02719899, NCT01143454, and NIH Clinical Center blood bank (NCT00001846).

Funding

This study was funded by the Division of Intramural Research of the NHLBI of the NIH (MNS).

## References

1. Johnson JB et al. Alternate day calorie restriction improves clinical findings and reduces markers of oxidative stress and inflammation in overweight adults with moderate asthma. Free radical biology & medicine 42, 665–674 (2007). [PubMed: 17291990]
2. Fraser DA et al. Reduction in serum leptin and IGF-1 but preserved T-lymphocyte numbers and activation after a ketogenic diet in rheumatoid arthritis patients. Clin Exp Rheumatol 18, 209–214 (2000). [PubMed: 10812493]
3. Traba J et al. Fasting and refeeding differentially regulate NLRP3 inflammasome activation in human subjects. The Journal of clinical investigation 125, 4592–4600 (2015). [PubMed: 26529255]
4. Meydani SN et al. Long-term moderate calorie restriction inhibits inflammation without impairing cell-mediated immunity: a randomized controlled trial in non-obese humans. Aging 8, 1416–1431 (2016). [PubMed: 27410480]
5. Sack MN Mitochondrial fidelity and metabolic agility control immune cell fate and function. The Journal of clinical investigation 128, 3651–3661 (2018). [PubMed: 30059015]
6. Han K et al. A Pilot Study To Investigate the Immune-Modulatory Effects of Fasting in Steroid-Naive Mild Asthmatics. Journal of immunology 201, 1382–1388 (2018).
7. Husebye H et al. Endocytic pathways regulate Toll-like receptor 4 signaling and link innate and adaptive immunity. EMBO J 25, 683–692 (2006). [PubMed: 16467847]
8. Crotzer VL & Blum JS Cytosol to lysosome transport of intracellular antigens during immune surveillance. Traffic 9, 10–16 (2008). [PubMed: 17916226]
9. Pasquale EB Eph-ephrin bidirectional signaling in physiology and disease. Cell 133, 38–52 (2008). [PubMed: 18394988]
10. Finak G et al. Standardizing Flow Cytometry Immunophenotyping Analysis from the Human ImmunoPhenotyping Consortium. Sci Rep 6, 20686 (2016). [PubMed: 26861911]
11. Langfelder P & Horvath S WGCNA: an R package for weighted correlation network analysis. BMC Bioinformatics 9, 559 (2008). [PubMed: 19114008]
12. Shoemaker JE et al. CTen: a web-based platform for identifying enriched cell types from heterogeneous microarray data. BMC Genomics 13, 460 (2012). [PubMed: 22953731]
13. Lee GR, Fields PE & Flavell RA Regulation of IL-4 gene expression by distal regulatory elements and GATA-3 at the chromatin level. Immunity 14, 447–459 (2001). [PubMed: 11336690]
14. Xiao H et al. HDAC5 controls the functions of Foxp3(+) T-regulatory and CD8(+) T cells. Int J Cancer 138, 2477–2486 (2016). [PubMed: 26704363]
15. Klemann C et al. Clinical and Immunological Phenotype of Patients With Primary Immunodeficiency Due to Damaging Mutations in NFKB2. Front Immunol 10, 297 (2019). [PubMed: 30941118]
16. Grant CE, Bailey TL & Noble WS FIMO: scanning for occurrences of a given motif. Bioinformatics 27, 1017–1018 (2011). [PubMed: 21330290]
17. Howell JJ & Manning BD mTOR couples cellular nutrient sensing to organismal metabolic homeostasis. Trends Endocrinol Metab 22, 94–102 (2011). [PubMed: 21269838]
18. Durant L et al. Diverse targets of the transcription factor STAT3 contribute to T cell pathogenicity and homeostasis. Immunity 32, 605–615 (2010). [PubMed: 20493732]
19. Traba J et al. Prolonged fasting suppresses mitochondrial NLRP3 inflammasome assembly and activation via SIRT3 mediated activation of Superoxide Dismutase 2. The Journal of biological chemistry 292, 12153–12164 (2017). [PubMed: 28584055]
20. Ciofani M et al. A validated regulatory network for Th17 cell specification. Cell 151, 289–303 (2012). [PubMed: 23021777]

21. Holloway AF, Rao S & Shannon MF Regulation of cytokine gene transcription in the immune system. Molecular immunology 38, 567–580 (2002). [PubMed: 11792425]
22. Vallabhapurapu S & Karin M Regulation and function of NF-kappaB transcription factors in the immune system. Annu Rev Immunol 27, 693–733 (2009). [PubMed: 19302050]
23. Smale ST Transcriptional regulation in the immune system: a status report. Trends Immunol 35, 190–194 (2014). [PubMed: 24703179]
24. Coffer PJ & Burgering BM Forkhead-box transcription factors and their role in the immune system. Nature reviews. Immunology 4, 889–899 (2004).
25. Hori S, Nomura T & Sakaguchi S Control of regulatory T cell development by the transcription factor Foxp3. Science 299, 1057–1061 (2003). [PubMed: 12522256]
26. Zhou W et al. FoxO4 inhibits NF-kappaB and protects mice against colonic injury and inflammation. Gastroenterology 137, 1403–1414 (2009). [PubMed: 19560465]
27. Baughman G, Wiederrecht GJ, Campbell NF, Martin MM & Bourgeois S FKBP51, a novel T-cell-specific immunophilin capable of calcineurin inhibition. Mol Cell Biol 15, 4395–4402 (1995). [PubMed: 7542743]
28. Zannas AS et al. Epigenetic upregulation of FKBP5 by aging and stress contributes to NF-kappaB-driven inflammation and cardiovascular risk. Proc Natl Acad Sci U S A 116, 11370–11379 (2019). [PubMed: 31113877]
29. Stechschulte LA et al. FKBP51 reciprocally regulates GRalpha and PPARgamma activation via the Akt-p38 pathway. Mol Endocrinol 28, 1254–1264 (2014). [PubMed: 24933248]
30. Pertea M, Kim D, Pertea GM, Leek JT & Salzberg SL Transcript-level expression analysis of RNA-seq experiments with HISAT, StringTie and Ballgown. Nature protocols 11, 1650–1667 (2016). [PubMed: 27560171]
31. Pertea M et al. StringTie enables improved reconstruction of a transcriptome from RNA-seq reads. Nature biotechnology 33, 290–295 (2015).
32. Frazee AC et al. Ballgown bridges the gap between transcriptome assembly and expression analysis. Nature biotechnology 33, 243–246 (2015).
33. Yu G, Wang LG, Han Y & He QY clusterProfiler: an R package for comparing biological themes among gene clusters. OMICS 16, 284–287 (2012). [PubMed: 22455463]
34. Warde-Farley D et al. The GeneMANIA prediction server: biological network integration for gene prioritization and predicting gene function. Nucleic Acids Res 38, W214–220 (2010). [PubMed: 20576703]
35. Lopes CT et al. Cytoscape Web: an interactive web-based network browser. Bioinformatics 26, 2347–2348 (2010). [PubMed: 20656902]
36. Taylor A, Steinberg J, Andrews TS & Webber C GeneNet Toolbox for MATLAB: a flexible platform for the analysis of gene connectivity in biological networks. Bioinformatics 31, 442–444 (2015). [PubMed: 25319962]

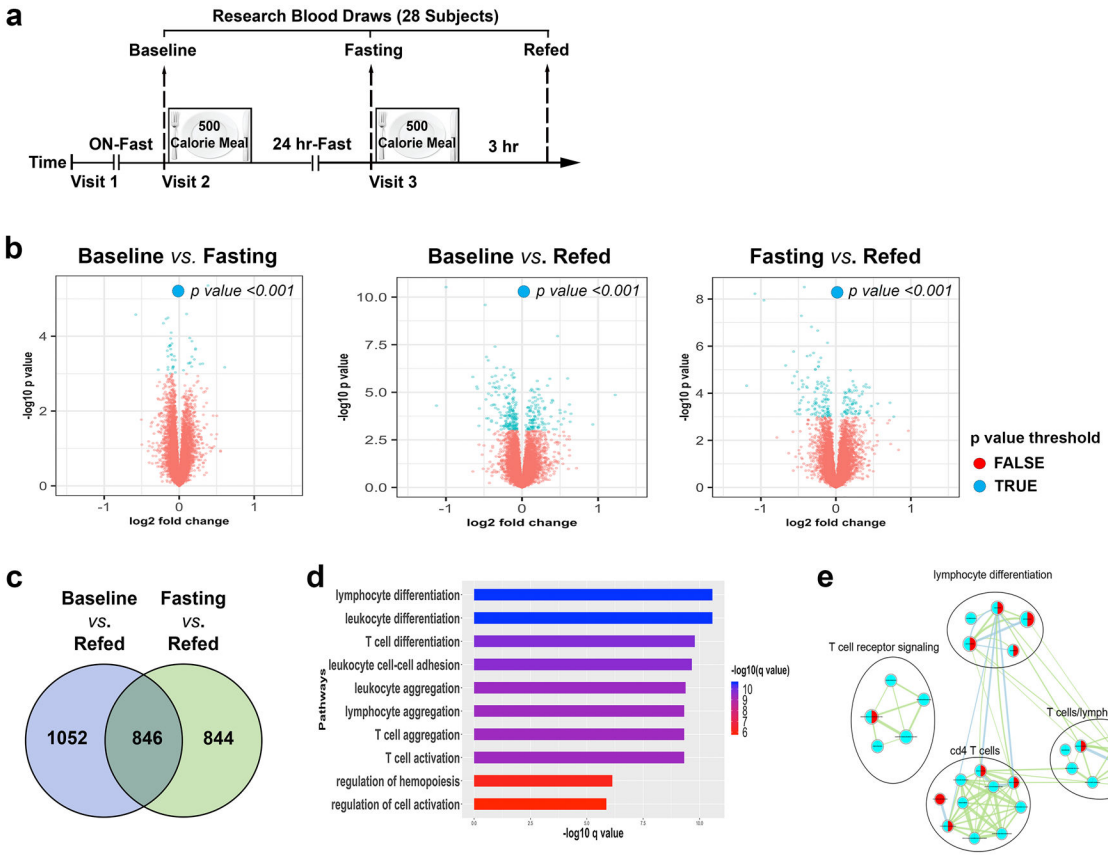


**FIGURE 1. RNAseq Analysis Shows Distinct Separation of the 3 Caloric-load Conditions.**

**a**, Schematic of the protocol showing intervals between fixed caloric meals and temporal research blood draws. The clinical protocol was established to perform immune cell profiling in 28 healthy human subjects. **b**, Volcano plots of all the genes in the indicated comparison is shown with DE genes. (p value threshold <0.001, colored as blue dots (Source Data: Statistical Source Data Fig. 1)). RNA sequencing was performed on PBMCs from 21 subjects following an overnight (baseline) and following a 24-hr. fast and 3 hrs. after refeeding. **c**, Venn diagram shows the number of overlapping versus distinct DE genes from baseline and 24-hr. fasting to refed comparisons. **d**, Top 10 pathways (q value<0.05, which depict p values adjusted for false discovery rates) from the pathway enrichment analysis of the 846 DE genes overlapping in the two comparisons (see Fig. 1C.). **e**, T cell specific differential pathway enrichment maps by overlaying the results of 24-hr. fasting *vs.* refed (green nodes) on top of the baseline *vs.* refed (red nodes) comparison. Each node represents distinct T cell processes or a pathway, and a single-colored node represents a pathway that was exclusively enriched by DE genes from one of the two comparisons. If common genes are annotated within two biological processes, then an edge connecting the two nodes is shown. The red and the teal-colored nodes represent pathways exclusively regulated by baseline or fasting respectively compared to refeeding. The bicolored nodes are regulated by both baseline and fasting *vs.* refeeding.

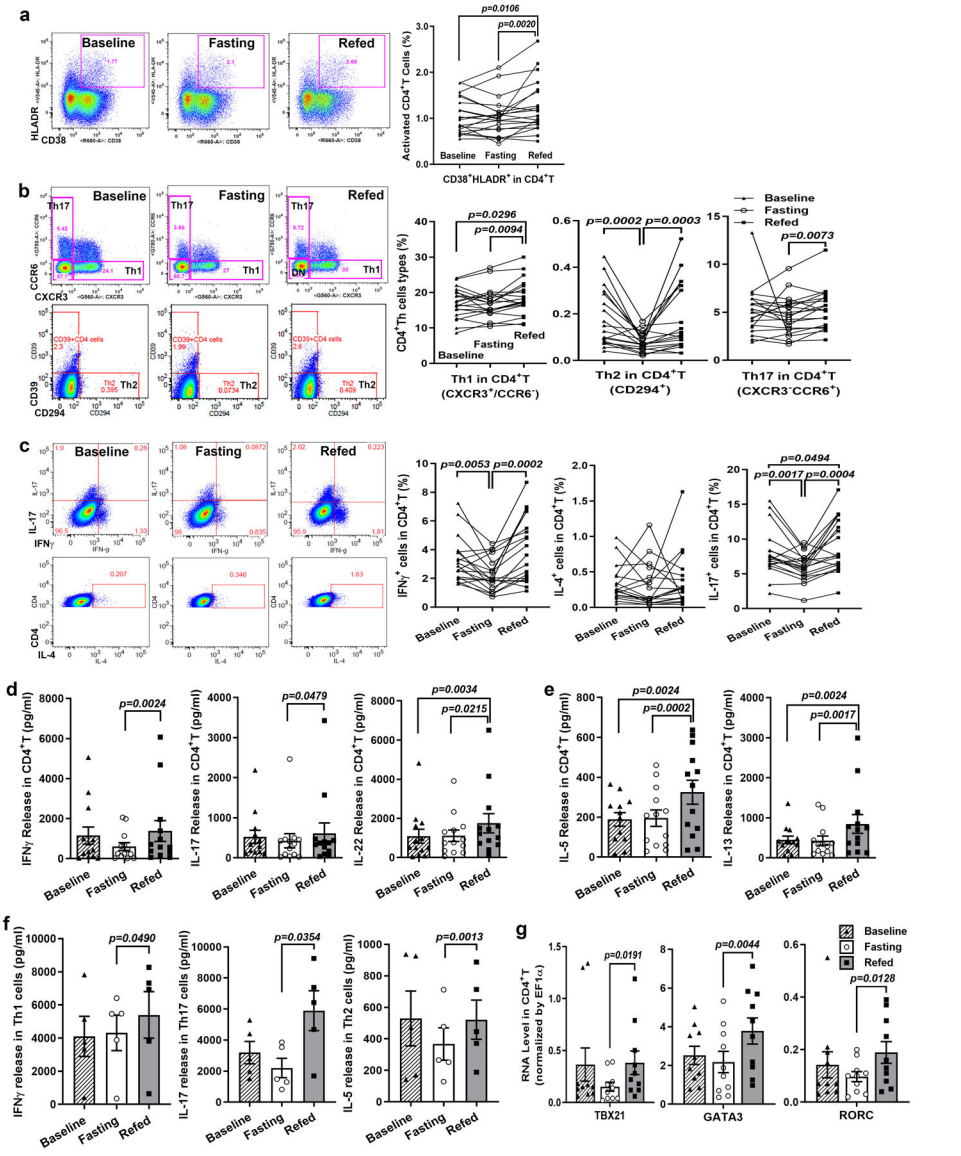


**FIGURE 2. Fasting/Feeding Differentially Regulate CD4$^+$ T Cell Activation and Differentiation.**

**a-c**, The dot-line plots show relative cell populations (percentiles, n=19 biologically independent subjects, Wilcoxon two-sided paired analysis). **a**, Representative flow plots of activated CD4$^+$ T cells (CD38$^+$HLADR$^+$) comparing PBMCs (baseline, 24-hr. fasting, and refed states). **b**, Comparing relative cell population frequencies with specific CD4$^+$ T cell surface markers. The plots show increased Th1 (CXCR3$^+$CCR6$^-$), Th17 (CXCR3$^-$CCR6$^+$), and Th2 (CD294$^+$) surface markers on refed PBMCs. **c**, Comparison of intracellular cytokine markers. The plots show increased (percentiles) of IFN$\gamma^+$ and IL-17$^+$ in refed cells (n=19 biologically independent subjects). **d-e**, ELISA measurement of cytokine release after CD4$^+$ T cell activation. Bar graphs (mean ± SEM with value of each subject, n=13, duplicate experiments, two-sided, Wilcoxon paired analysis after normalization). **d**, Release of IFN, IL-17, IL-22, **e**, IL-5 and IL-13 from baseline, 24-hr. fasted and refed CD4$^+$ T cells. **f**, Following Th-subpopulation differentiation IFN$\gamma$, IL-5 and IL-17 secretion were measured

from Th1, Th2 cells and Th17 cells respectively. Bar graphs (mean ± SEM with data points for each subject, n=5 duplicate experiments, two-sided, ratio paired Student's t-test). **g**, Relative mRNA levels of Th1 (TBX21), Th2 (GATA3) and Th17 (RORC) canonical TFs in fasted *vs.* refed $CD4^+$ T cells. Bar graphs represent mean ± SEM with each value 3–4 replicates (n=10 biological distinct subjects, two-sided paired Student's t-test). Supplementary Data1for Fig.2 shows flow cytometry gating strategy.

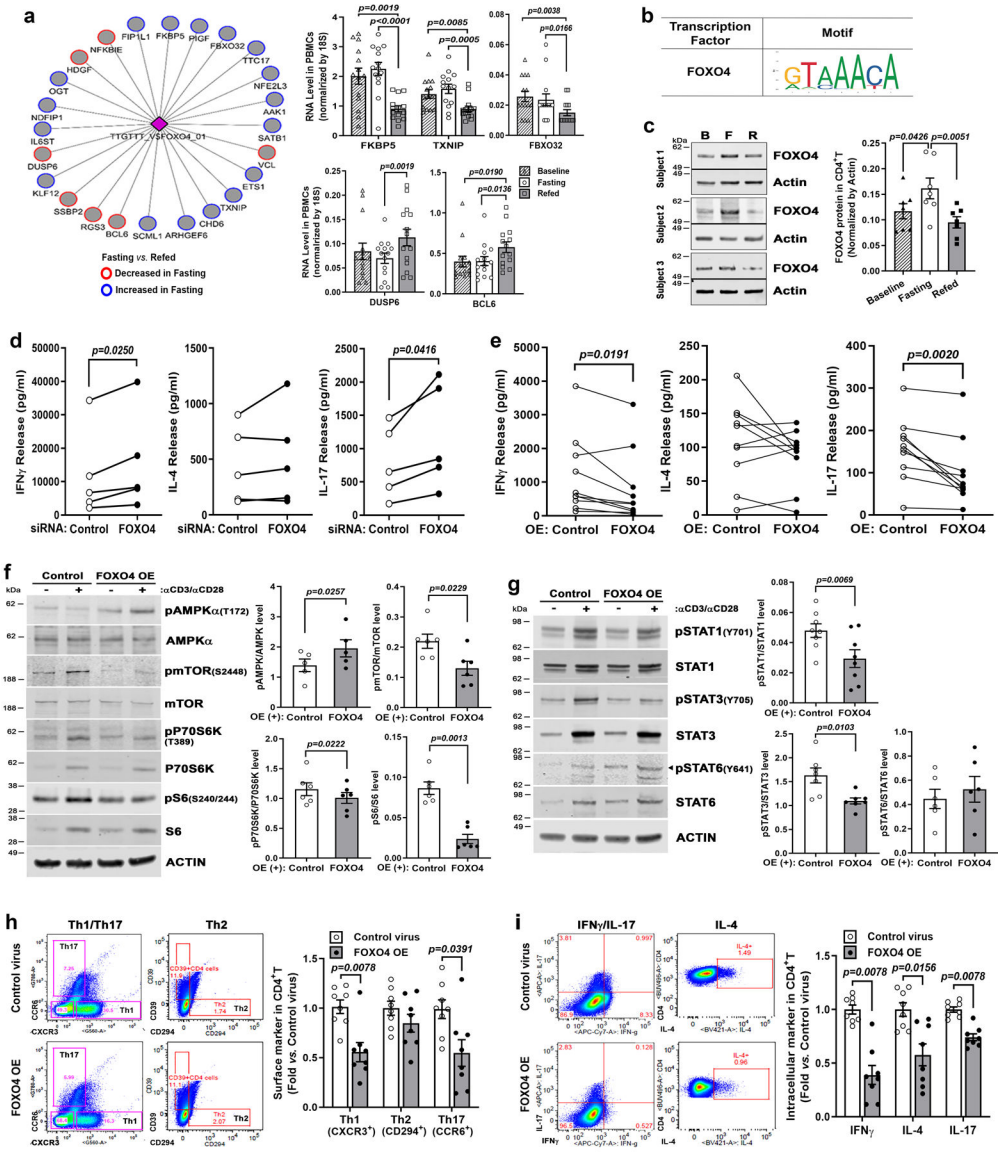

**FIGURE 3. Fasting-induced FOXO4 Effects.**

**a**, FOXO4 transcription network and its targets identified by GeneMANIA analysis. The 24-hr. fasting DE genes (circular nodes) show fold increased (blue circles) or decreased (red circles) expression relative to refeeding levels. Validation of target relative genes transcript levels by qRT-PCR in PBMCs (bar plots mean ± SEM with mean values of 3–4 replicates from n=14 subjects, two-sided, paired Student's t-test). **b**, Concurrent analysis using the Find Individual Motif Occurrences (FIMO) tool identified the FOXO4 binding motif in the promoter regions of a significant proportion of fasted DE upregulated genes (fisher exact test for FOXO4 motif enrichment significance, p=0.049). **c**, Representative protein blots from 3 subjects (left panel) and quantitative changes (right panel) of FOXO4 levels in $CD4^+$ T cells from the 3 caloric-load states. (Bar graph mean ± SEM, n=7 subjects, two-sided, paired Student's t-test). **d-e**, Cytokine release of IFN**γ**, IL-4 and IL-17 following FOXO4 knockdown (KD) and overexpression in activated $CD4^+$ T cells. The cytokine release of KD

cells measured (n=5 separate experiment **(d)**) or from FOXO4-overexpressed cells (n=10 separate experiments **(e)**) using two-sided, paired Student's t-test analysis. The dot and line plots show the mean value of each subject and the values represent the average of duplicate experiments. Statistical analysis using two-sided, paired Wilcoxon test. f-g, Representative protein blot (left panel) and quantification (right panel) comparing transduction of control *vs.* FOXO4 lentivirus (OE) with (+) or without (−) $CD4^+$ T cell activation (two-sided, paired Student's t-test). **f**, mTOR signaling pathway phosphorylation and total protein kinase levels (Bar graphs - mean ± SEM of n=6 biologically independent subjects). **g**, STAT signaling proteins (Bar graphs - mean ± SEM of 6–8 biologically independent subjects). **h-I**, Flow cytometric plots of cell surface; Th1 ($CXCR3^+CCR6^-$), Th17 ($CXCR3^-CCR6^+$), and Th2 ($CD294^+$) and intracellular; IFN**γ**, IL-17, and IL-4, markers from healthy volunteer $CD4^+$ T cells transduced with control or FOXO4 lentivirus (Bar graphs - mean ± SEM from n=8 subjects, two-sided, paired Wilcoxon test). Supplementary Data2 for Fig.3 shows flow cytometry gating strategy.

Source Data Fig.3 Unprocessed immunoblots.

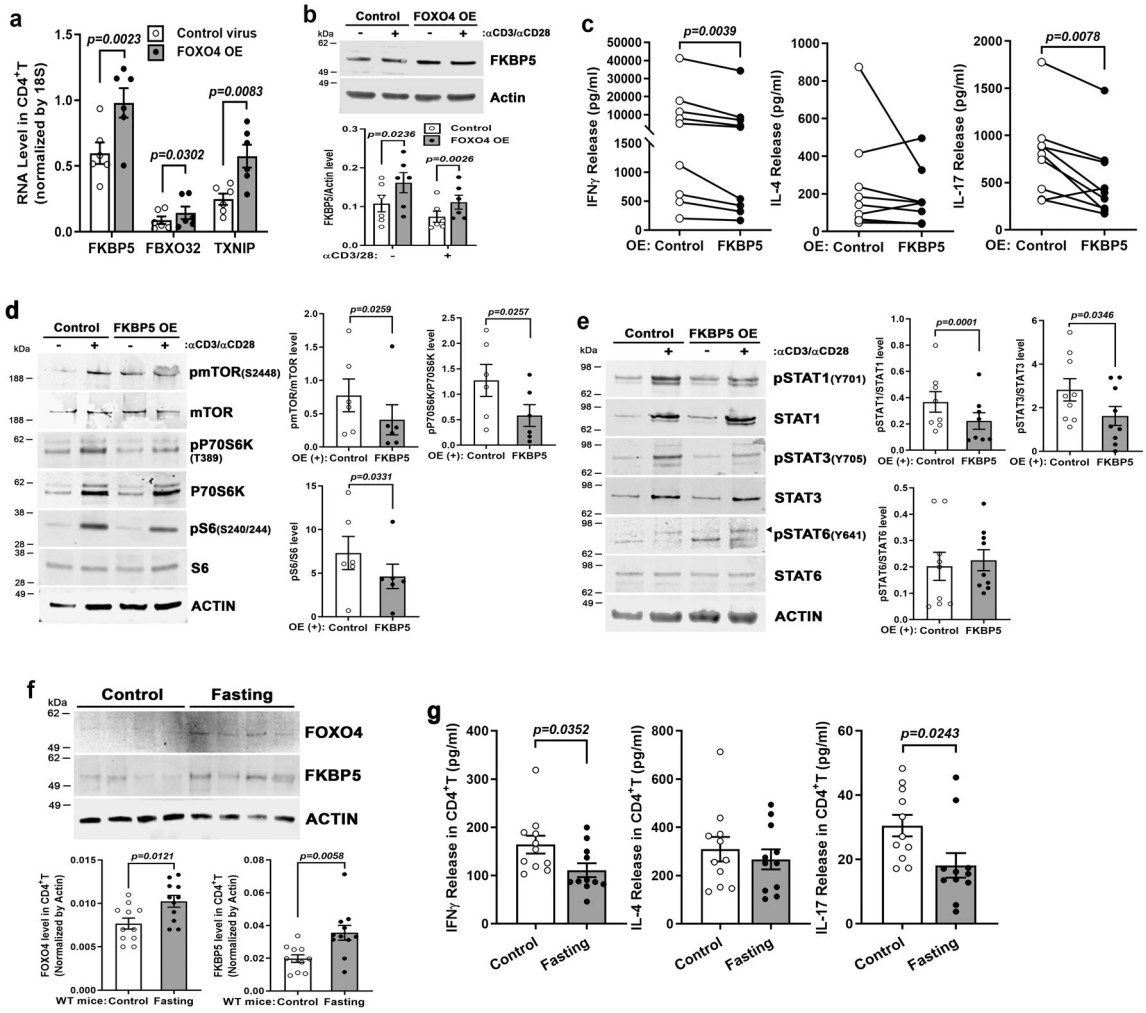


**FIGURE 4. FKBP5 Induction Mimics FOXO4 overexpression and Fasting effects on Th Cell Activation.**

**a**, RT-PCR analysis of FOXO4 target genes following FOXO4 transduction in $CD4^+$ T cells (Bar graphs - mean ± SEM from duplicate experiments in n=6 biologically independent subjects, two-sided, paired Student's t-test). **b**, Representative protein blot of FKBP5 (top panel) and quantification (bottom panel) comparing transduction of control *vs.* FOXO4 lentivirus (OE) with (+) and without (−) $CD4^+$ T cell activation (Bar graphs - mean ± SEM of n=6 subjects, two-sided, paired Student's t-test). **c**, Cytokine release of IFNγ, IL-4 and IL-17 following FKBP5-overexpression in activated $CD4^+$ T cells from n=9 subjects). The dot and line plots show the mean value of each subject. The values represent the average of duplicate experiments. Statistical analysis using two-sided, paired Wilcoxon test. **d-e**, Representative protein blot (left panel) and quantification (right panel) comparing transduction of $CD4^+$ T cells with control *vs.* FKBP5 lentivirus (OE) with (+) or without (−) TCR activation (Bar graph - mean ± SEM value of subjects. **d**, mTOR signaling pathway phosphorylated and total protein kinase levels are shown (n=6 biologically independent experiments, two-sided, paired Student's t-test compared to vector controls). **e**, STAT signaling proteins (n=8–9 biologically independent experiments, two-sided, paired Student's

t-test compared to vector controls). pSTAT1/STAT1 (n=8); pSTAT3/STAT3 (n=9); pSTAT6/STAT6 (n=9). **f**, Representative protein blot (top panel) and quantitative changes (bottom panel) in mouse $CD4^+$ T cells obtained from fed- or 48-hr. fasted-mice. Protein level of FOXO4 and FKBP5 in mouse $CD4^+$ T cells after 24-hr. TCR activation (Bar graph - mean ± SEM of n=11 mice per group, two-sided, unpaired Student's t-test). **g**, The cytokine release in fed or fasted mouse $CD4^+$ T cells. The histogram shows mean ± SEM levels from n=11 mice from duplicate assays (two-sided, unpaired Student's t-test).
Source Data Fig.4 Unprocessed immunoblots.

## KEY RESOURCES TABLE

| REAGENT or RESOURCE | SOURCE | IDENTIFIER |
|---|---|---|
| **Antibodies** | | |
| Mouse monoclonal anti-ACTIN | Millipore | Cat. MAB1501; RRID:AB_2223041 |
| Rabbit polyclonal anti-AMPKα | Cell Signaling | Cat. #2532S; RRID:AB_330331 |
| Rabbit polyclonal anti-p-AMPKα (T172) | Cell Signaling | Cat. #2535S; RRID:AB_331250 |
| Rabbit polyclonal anti-FKBP5 | Cell Signaling | Cat. #12210S; RRID:AB_2797846 |
| Rabbit polyclonal anti-FOXO4 | Cell Signaling | Cat. #9472S; RRID:AB_10831833 |
| Rabbit polyclonal anti-FOXO4 | Abcam | Cat. AB63254; RRID:AB_1140571 |
| Rabbit monoclonal anti-mTOR | Cell Signaling | Cat. #2983S; RRID:AB_2105622 |
| Rabbit polyclonal anti-p-mTOR (S2448) | Cell Signaling | Cat. #2971S; RRID:AB_330970 |
| Rabbit polyclonal anti-P70S6K | Cell Signaling | Cat. #9202S; RRID:AB_331676 |
| Rabbit polyclonal anti-p-P70S6K (T389) | Cell Signaling | Cat. #9205S; RRID:AB_330944 |
| Mouse monoclonal anti-S6 | Cell Signaling | Cat. #2317S; RRID:AB_2238583 |
| Rabbit monoclonal anti-pS6 (S240/244) | Cell Signaling | Cat. #5364S; RRID:AB_10694233 |
| Rabbit monoclonal anti-STAT1 | Cell Signaling | Cat. #14994S; RRID:AB_2737027 |
| Rabbit monoclonal anti-p-STAT1 (Y701) | Cell Signaling | Cat. #9167S; RRID:AB_561284 |
| Rabbit monoclonal anti-STAT3 | Cell Signaling | Cat. #12640S; RRID:AB_2629499 |
| Rabbit monoclonal anti-p-STAT3 (Y705) | Cell Signaling | Cat. #9145S; RRID:AB_2491009 |
| Rabbit monoclonal anti-STAT6 | Cell Signaling | Cat. #5397S; RRID:AB_11220421 |
| Rabbit polyclonal anti-p-STAT6 (Y641) | Cell Signaling | Cat. #9361S; RRID:AB_331595 |
| Rabbit monoclonal anti-TBX21 | Cell Signaling | Cat. #13232; RRID:AB_2616022 |
| Mouse monoclonal anti-GATA3 | Cell Signaling | Cat. #5852; RRID:AB_10835690 |
| Rat monoclonal anti-RORC | ThermoFisher Scientific | Cat. #14-6988-82; RRID: AB_1834475 |
| Mouse monoclonal anti-human CD3 | Biolegend | Cat. #317326; RRID:AB_11150592 |
| Mouse monoclonal anti-human CD28 | Biolegend | Cat. #302934; RRID:AB_11148949 |
| Mouse monoclonal anti-IFNγ | eBioscience | Cat. #16731885; RRID:AB_469251 |
| Mouse monoclonal anti-IL-4 | eBioscience | Cat. #16704885; RRID:AB_469211 |
| Hamster anti-mouse CD3 | Biolegend | Cat. #100340; RRID:AB_11149115 |
| Hamster anti-mouse CD28 | Biolegend | Cat. #102116; RRID:AB_11147170 |
| IRDye800CW Goat anti-rabbit IgG | Li-Cor Bioscience | Cat. #926–32211, RRID:AB_621843 |
| IRDye680RD Donkey anti-mouse IgG | Li-Cor Bioscience | Cat. #926–68072, RRID: AB_10954628 |
| IRDye680RD Goat anti-rabbit IgG | Li-Cor Bioscience | Cat. #926–68071, RRID: AB_10956166 |
| **Bacterial and Virus Strains** | | |
| One Shot TOP10 *E. coli* | ThermoFisher Scientific | Cat. C404003 |

| REAGENT or RESOURCE | SOURCE | IDENTIFIER |
|---|---|---|
| pLenti-c-Myc-DDK | Origene Technologies | Cat. PS1000064 |
| pLenti-c-Myc-DDK-FOXO4 | Origene Technologies | Cat. RC213185L1 |
| pLenti-c-mGFP | Origene Technologies | Cat. PS100071 |
| pLenti-c-mGFP-FOXO4 | Origene Technologies | Cat. RC213185L2 |
| pLVX-IRES-GFP | This paper | N/A |
| pLVX-FKBP5-IRES-GFP | This paper | N/A |
| **Biological Samples** | | |
| Human serum | From subject cohort - ClinicalTrials.gov ID-NCT02719899 | N/A |
| **Chemicals, Peptides, and Recombinant Proteins** | | |
| PMA | Sigma Aldrich | Cat. P8139 |
| Ionomycin | Sigma Aldrich | Cat. I0634 |
| Cell Stimulation Cocktail plus Protein Transport Inhibitors | eBioscience | Cat. 00-4975-03 |
| Brefeldin A | Biolegend | Cat. 420601 |
| DEAE-Dextran | Sigma Aldrich | Cat. D9885 |
| Human IL-2 Recombinant protein | Peprotech | Cat. 200–02B |
| Human IL-4 Recombinant protein | Peprotech | Cat. 200–04B |
| Human IL-6 Recombinant protein | Peprotech | Cat. 200–06B |
| Human IL-12 Recombinant protein | Peprotech | Cat. 200–12B |
| Human IL-23 Recombinant protein | Peprotech | Cat. 200–23B |
| Human TGF-β1 Recombinant protein | Peprotech | Cat. 100–21B |
| Human IL-1ββRecombinant protein | Peprotech | Cat. 200–01B |
| **Critical Commercial Assays** | | |
| Lyoplate Stain 175<br>See Suppl. Table 1 for Flow Cytometry Panel | BD | Mat. 624215, Lot. 5260872 |
| Compensation Plate Stain 177 | BD | Mat. 624217, Lot. 5260875 |
| CyQuant Cell Proliferation Assay | Invitrogen | Cat. C7026 |
| Human IFNγβDuoset ELISA Kit | R&D Systems | Cat. DY285B |
| Human IL-4 Duoset ELISA Kit | R&D Systems | Cat. DY204 |
| Human IL-5 Duoset ELISA Kit | R&D Systems | Cat. DY205 |
| Human IL-13 Duoset ELISA Kit | R&D Systems | Cat. DY213 |
| Human IL-17 Duoset ELISA Kit | R&D Systems | Cat. DY317 |
| Human IL-22 Duoset ELISA Kit | R&D Systems | Cat. DY782 |
| Mouse IFNγβDuoset ELISA Kit | R&D Systems | Cat. DY485 |
| Mouse IL-4 Duoset ELISA Kit | R&D Systems | Cat. DY404 |
| Mouse IL-17 Duoset ELISA Kit | R&D Systems | Cat. DY421 |
| **Deposited Data** | | |
| Raw and analyzed data | This paper | GEO database: https://www.ncbi.nlm.nih.gov/geo/query/acc.cgi?acc=GSE165149<br>Codes: https://github.com/NHLBI-BCB/PTNA |

| REAGENT or RESOURCE | SOURCE | IDENTIFIER |
|---|---|---|
| Human reference genome NCBI build 37, GRCh37 | Genome Reference Consortium | http://www.ncbi.nlm.nih.gov/projects/genome/assembly/grc/human/ |
| **Experimental Models: Cell Lines** | | |
| HEK293T | Dr. Toren Finkel's Lab | N/A |
| **Experimental Models: Organisms/Strains** | | |
| Human Healthy Volunteer | NIH Clinical Center Blood Bank (NCT00001846) and ClinicalTrials.gov ID-NCT01143454 | N/A |
| **Oligonucleotides** | | |
| Human TBX21 | Integrated DNA Technologies | F: CGTGACTGCCTACCAGAAT<br>R: ATCTCCCCCAAGGAATTGAC |
| Human GATA3 | Integrated DNA Technologies | F: GAACCGGCCCCTCATTAAG<br>R: ATTTTTCGGTTTCTGGTCTGGAT |
| Human RORC | Integrated DNA Technologies | F: GCATGTCCCGAGATGCTGTC<br>R: CTGGGAGCCCCAAGGTGTAG |
| Human EF1a | Integrated DNA Technologies | F: GTTGATATGGTTCCTGGCAAGC<br>R: GCCAGCTCCAGCAGCCTTC |
| QuantiTech Primer Assays | Qiagen | N/A |
| Accell Non-targeting Control | Dharmacon | Cat. D-001910-01-20 |
| SMARTpool: Accell FOXO4 | Dharmacon | Cat. E-003016-00-0010 |
| SMARTpool: Accell FKBP5 | Dharmacon | Cat. E-004224-00-0010 |
| **Recombinant DNA** | | |
| psPAX2 | Addgene | Cat. 12260 |
| pMD2.G | Origene Technologies | Cat. 12259 |
| pCMV6-Entry-c-Myc-DDK | Origene Technologies | Cat. PS100001 |
| pCMV6-Entry-c-Myc-DDK-FOXO4 | Origene Technologies | Cat. RC213185 |
| pCMV3-C-Flag | Sino Biological Inc. | Cat. CV012 |
| pCMV3-C-FKBP5-Flag | Sino Biological Inc. | Cat. HG11487-CF |
| **Software and Algorithms** | | |
| GraphPad PRIZM7 | NIH | N/A |
| Image Studio | Li-Cor Biosciences | N/A |
| FlowJo 9.9.6 | FlowJo | N/A |
| FastQC | http://www.bioinformatics.babraham.ac.uk/projects/fastqc | N/A |
| HISAT2 | https://daehwankimlab.github.io/hisat2/ | NA |
| Trimmomatic | https://github.com/timflutre/trimmomatic | |
| Stringtie | https://github.com/gpertea/stringtie | NA |
| Ballgown | http://bioconductor.org/packages/release/bioc/html/ballgown.html | NA |
| WGCNA | https://cran.r-project.org/web/packages/WGCNA/index.html | NA |
| ClusterProfiler | https://bioconductor.org/packages/release/bioc/html/clusterProfiler.html | N/A |
| R and R Studio | http://www.r-project.org/ | N/A |

| REAGENT or RESOURCE | SOURCE | IDENTIFIER |
|---|---|---|
| Cytoscape 3.7.2 | http://cytoscape.org/ | N/A |
| GeneNet tool box | http://avigailtaylor.github.io/gntat14 | N/A |
| Find Individual Motif Occurrences | http://meme-suite.org/doc/fimo.html | N/A |
| PLS-DA | https://bioconductor.org/packages/mixOmics/ | |
| **Other** | | |
| Lymphocyte Separation Medium | MP Biomedicals | Cat. 0850494 |
| Human $CD4^+$ T Cell Isolation Kit | Miltenyi Biotec | Cat. 130-096-533 |
| Mouse $CD4^+$ T Cell Isolation Kit | Miltenyi Biotec | Cat. 130-104-454 |
| miRNeasy Micro Kit | Qiagen | Cat. 217084 |
| TruSeq Stranded Total RNA HT Kit | Illumina | Cat. 20020595 |
| Human T cell Nucleofector kit | Lonza | Cat. VVPA-1002 |
| Accell siRNA Delivery Media | Dharmacon | Cat. B-005000–100 |
| Polyjet In Vitro DNA Transfection Reagent | Signagen Laboratories | Cat. SL100688 |
| NucleoSpin RNA Kit | Macherey-Nagel | Cat. 740955 |
| First-strand Synthesis SuperMix | Invitrogen | Cat. 11752250 |
| FastStart Essential DNA Green Master Mix | Roche Life Science | Cat. 06924204001 |
| ImmunoCult Human CD3/CD28 T Cell Activator | Stemcell | Cat. 10971 |
| Trans-Blot Turbo Nitrocellulose Transfer Packs | Bio-Rad | Cat. 1704158 |
| Live/Dead Fixable Yellow Dead Cell Stain Kit | Invitrogen | Cat. L34968 |